Article:
Du, J., Jiang, X., Wang, T. et al. (4 more authors) (2025) Optimization of mix design for controlled low-strength material produced from red-bed mudstone. Construction and Building Materials, 493. 143280. ISSN: 0950-0618

https://doi.org/10.1016/j.conbuildmat.2025.143280

Optimization of mix design for controlled low-strength material produced from red-bed mudstone

Jianbiao Du
1. School of Civil Engineering, Southwest Jiaotong Univ., Chengdu 610031, China
E-mail: 1781950412@qq.com

Xin Jiang*
1. School of Civil Engineering, Southwest Jiaotong Univ., Chengdu 610031, China;
2.
E-mail:

Tengfei Wang
1. School of Civil Engineering, Southwest Jiaotong Univ., Chengdu 610031, China;
2. MOE Key Laboratory of High-speed Railway Engineering, Southwest Jiaotong Univ., Chengdu 610031, China
E-mail: w@swjtu.edu.cn; ORCID: 0000-0003-4079-0687

Qiang Luo
1. School of Civil Engineering, Southwest Jiaotong Univ., Chengdu 610031, China;
2. MOE Key Laboratory of High-speed Railway Engineering, Southwest Jiaotong Univ., Chengdu 610031, China
E-mail: lqrock@swjtu.edu.cn

David P. Connolly
3. School of Civil Engineering, Univ. of Leeds, Leeds LS2 9JT, UK
Email: D.Connolly@leeds.ac.uk

Liang Zhang
1. School of Civil Engineering, Southwest Jiaotong Univ., Chengdu 610031, China;
2. MOE Key Laboratory of High-speed Railway Engineering, Southwest Jiaotong Univ., Chengdu 610031, China
E-mail: LZhang@swjtu.edu.cn

Qiuhui Hu
1. School of Civil Engineering, Southwest Jiaotong Univ., Chengdu 610031, China
E-mail: hqh@my.swjtu.edu.cn

Van Duc Nguyen

Abstract: Certain geotechnical materials such as red-bed mudstone have the propensity to disintegrate and soften upon water exposure. If used for construction, they can result in instability and deformation, and therefore are commonly replaced with imported sand and gravel. As a solution to this non-sustainable practice, this study proposes transforming red-bed mudstone into a Controlled Low-Strength Material (CLSM) blended with polycarboxylate superplasticizer. The newly proposed mix is studied, by varying the cement-to-soil ratio (*C*), water-to-solids ratio (*W*), and volume of polycarboxylate superplasticizer (*P*). The effect on the fresh CLSM mix (flowability, bleeding rate, setting time), hardened CLSM mix (settlement rate, compressive strength), and CLSM durability (drying shrinkage rate, water stability) are investigated. It is found that in the absence of polycarboxylate superplasticizer, increasing water content improves flowability but weakens the hardened mix and negatively effects durability. To overcome this, increased cement content is needed to ensure stability of the hardened mix and it's durability. However, with the addition of polycarboxylate superplasticizer, water content can be reduced without compromising engineering performance, thereby decreasing cement consumption. More specifically, increasing polycarboxylate superplasticizer reduces the water demand needed to achieve target flowability, resulting in lower bleeding, settlement and drying shrinkage rates, and improved compressive strength and water stability. In conclusion, the study demonstrates a pathway to repurpose red-bed mudstone waste, potentially turning an environmental liability into a usable asset for the construction industry.

Keywords: Red-bed mudstone recycling; Controlled Low-Strength Material (CLSM); Polycarboxylate superplasticizer; Sustainable construction materials; Waste utilization; Backfill applications; Engineering property enhancement

1. Introduction

Red-bed mudstone poses significant challenges in civil engineering due to its propensity to disintegrate and soften upon water exposure, leading to substantial strength reduction and compromised engineering performance (Aehnelt et al., 2021; Xu and Tang, 2023). Construction projects in areas rich in red-bed mudstone frequently grapple with issues such as slope instability, subgrade deformation, and pavement cracking (Cheng et al., 2004; Lei et al., 2019). In China, red-bed mudstone is extensively distributed across southeastern, northwestern, and southwestern regions, with the Sichuan Basin, spanning 165,000 km^2, serving as a representative area in the southwest (Pan and Peng, 2015). The humid and wet climate of this region exacerbates engineering failures, exemplified by the Bazhong to Guang'an Expressway project, which encountered 192 landslides due to red-bed mudstone, with remediation costs exceeding 55 million USD (Cheng et al., 2016). Internationally, regions such as western Kyushu (Japan), northwestern India, western United States, northern Chile, central and southern South Africa, and Western Australia face similar challenges posed by red-bed mudstone (Aehnelt et al., 2021; Pan and Peng, 2015).

To mitigate disaster risks associated with red-bed mudstone, excavated material is often discarded during infrastructure projects, with sand and gravel used as alternative backfill materials (Du et al., 2024; Hu et al., 2024). However, this practice significantly increases transportation costs and is in conflict with modern environmental standards which typically aim to maximise the reuse of indigenous site-won materials. Further, the disposal of waste red-bed mudstone occupies additional land, and excessive accumulation heightens the risk of landslides (Arm et al., 2017; Duan et al., 2019). Additionally, overextraction of natural sand and gravel accelerates vegetation degradation and ecological imbalance (Zhang et al., 2020). Backfilling projects with limited working spaces, such as

pipe galleries, bridge abutment backs, culvert backs, and retaining wall backs, present further challenges due to the difficulty of compacting traditional sand and gravel materials in confined areas (ACI, 1999).

In response to these challenges, transforming red-bed mudstone waste into Controlled Low-Strength Material (CLSM) presents a promising solution. CLSM, defined by the American Concrete Institute (ACI 229) as a self-compacting, flowable material requiring no compaction, offers advantages, including ease of placement, reduced labor, and suitability for confined spaces (Chang and Chen, 2006; Jian et al., 2022; Qian et al., 2019). Traditionally composed of fine aggregates, cement, and water, CLSM can incorporate additives like polycarboxylate superplasticizer and air-entraining agents to tailor its properties (ACI, 1999) to the desired application. By using waste red-bed mudstone as an aggregate in CLSM, it is possible to address disposal issues while reducing reliance on natural sand and gravel, thus aligning with sustainable construction practices.

However, the production of cement, a key component of CLSM, consumes non-renewable resources and generates greenhouse gas emissions, particularly CO_2 (Carrasco et al., 2019). Thus, excessive cement usage can undermine the economic and environmental benefits of CLSM. Consequently, there is a growing emphasis on adopting low-cost, energy-efficient, and environmentally friendly materials in CLSM production (Wang et al., 2023). Researchers have explored the partial or full replacement of cement with industrial by-products such as slag, cement kiln dust, rice husk ash, and stainless steel reduction slag to reduce costs and carbon emissions (Dalal et al., 2023; Sheen et al., 2013; Wu and Tsai, 2009). Additionally, industrial waste materials like dewatered sludge, waste glass, industrial incineration bottom ash, and rubber particles have been investigated as fine aggregate replacements, enhancing resource efficiency and sustainability (Kim et al., 2020; Zhang

et al., 2018).

Despite these advancements, limited research has explored the feasibility of using soils with poor engineering properties, such as red-bed mudstone, as aggregates in CLSM (Nataraja and Nalanda, 2008). Concerns persist that such soils may result in undesirable CLSM characteristics, for example affecting flowability and stability (ACI, 1999). Achieving adequate flowability with soil-based CLSM often requires high water content, leading to increased bleeding and settlement rates, and necessitating higher cement proportions to meet strength and durability requirements, factors that can erode the economic and environmental advantages of CLSM (ACI, 1999; Du et al., 2024; Hu et al., 2024).

To address these challenges, incorporating polycarboxylate superplasticizer, a widely used high-performance water reducer, offers a viable solution. Polycarboxylate superplasticizers effectively lower the water demand to achieve desired flowability, mitigating the adverse effects of increased water content (Wang et al., 2024). Previous studies have demonstrated that adding polycarboxylate superplasticizer enhances the flowability of CLSM prepared with excavated waste soils or dredged clays (Wan et al., 2023; Zhang et al., 2023). However, most existing research focuses primarily on flowability, with limited investigation into the effects of the quantity of polycarboxylate superplasticizer on other critical properties such as settlement rate, compressive strength, and durability (Wang et al., 2024).

This study investigates the feasibility of using waste red-bed mudstone as an aggregate in CLSM, enhanced with polycarboxylate superplasticizer. The aim of using polycarboxylate superplasticizer is to reduce water and cement requirements, improve performance, and contribute to sustainable development objectives. To do so, the effects of cement-to-soil ratio, water-to-solids ratio, and volume of polycarboxylate superplasticizer on the fresh, hardened, and durability properties of CLSM, are

studied.

2. Materials and Methods

To investigate the feasibility of using red-bed mudstone waste in CLSM production and to assess the impact of cement content, water ratio, and polycarboxylate superplasticizer on its properties, an experimental program was designed. The following sections describe the materials employed, the mix proportions formulated, and the testing methods used to evaluate the fresh, hardened, and durability characteristics of the CLSM mixtures.

2.1 Materials

The red-bed mudstone was sourced from a road construction site in suburban Chengdu, Sichuan Province. The XRD (X-Ray Diffraction) pattern (Fig. 1) indicates that the primary mineral components are quartz, muscovite, calcite, and chlorite. The basic physical properties and the particle size distribution curve are presented in Table 1 and Fig. 2, respectively. With a liquid limit below 50% and a plasticity index of 14.4, the red-bed mudstone is classified as low liquid limit clay under the *Unified Soil Classification System* (ASTM-D2487-17).

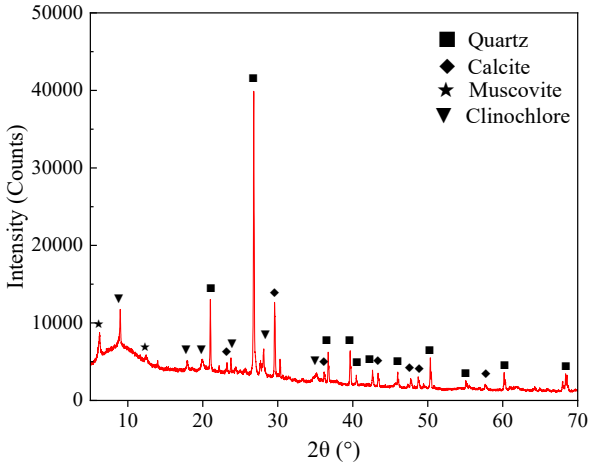

Fig. 1. X-ray diffraction patterns of the red-bed mudstone showing mineral composition.

Table 1. Index properties of red-bed mudstone.

Index property	Value	Unit

Appearance	Maroon colored	-
Specific gravity	2.696	-
Maximum dry density	1.95	g/cm^3
Optimum moisture content (OMC)	10.65	%
Liquid limit (LL)	31.5	%
Plasticity index (PI)	14.4	-
Particles < 75 μm	78.9	%
Free swelling ratio	14.92	%
Standard moisture absorption	0.86	%

The P042.5 composite Portland cement (OPC) used in this study primarily comprises SiO_2, Fe_2O_3, Al_2O_3, and CaO. The initial and final setting times were 182 min and 249 min, respectively, with all other properties meeting the requirements of the Chinese standard GB175-2007. The particle size distribution curve, obtained using a Malvern Mastersizer 2000 laser particle size analyser, is shown in Fig. 2.

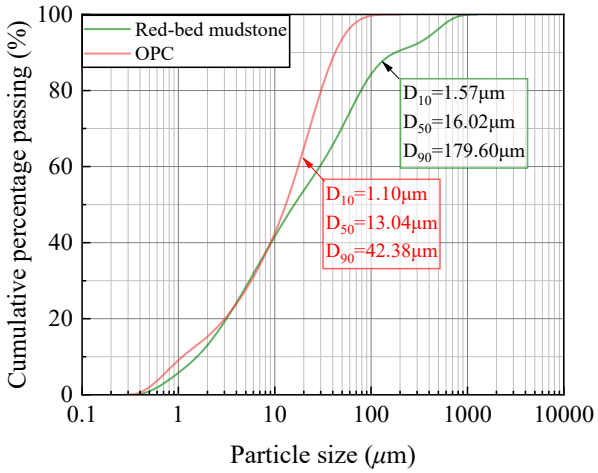

Fig. 2. Particle size distributions of red-bed mudstone and OPC.

The polycarboxylate superplasticizer used in this study, designated as ZK-1, was supplied by Jizhou Yasidun Building Materials Technology Co., Ltd. (China). The polycarboxylate superplasticizer appears as a white granular powder, as shown in Fig. 3(a). Scanning Electron Microscopy (SEM) analysis (Fig. 3(b)) revealed its granular morphology. Energy-Dispersive Spectroscopy (EDS) was used to analyse the surface composition of the polycarboxylate superplasticizer particles, with results shown in Fig. 4. The primary surface elements identified were C, O, and S. In addition, standard tap

water was used throughout the experiments.

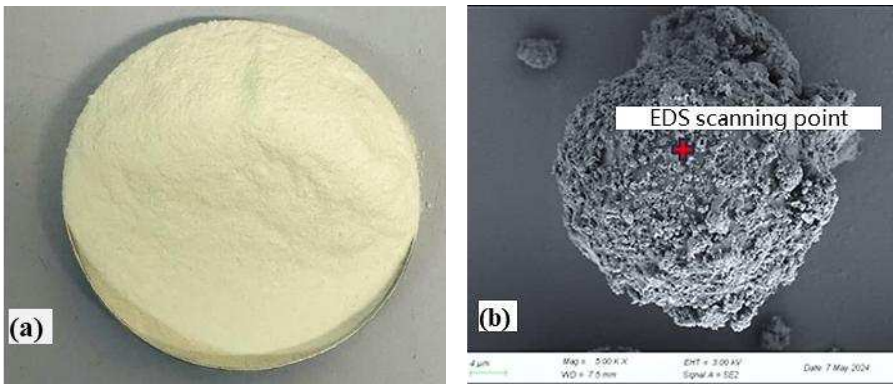

Fig. 3. Morphology of polycarboxylate superplasticizer: (a) macroscopic view; (b) microscopic view.

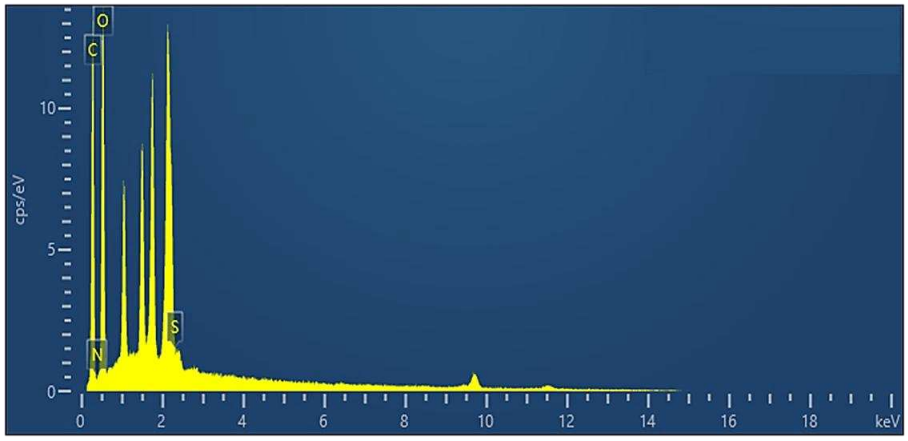

Fig. 4. EDS analysis of polycarboxylate superplasticizer revealing elemental composition.

2.2 Mix Proportions

In the experiment, the following ratios are defined:

1. The ratio of the mass of cement to the mass of soil particles. Termed the cement-to-soil ratio (*C*).
2. The ratio of the mass of the polycarboxylate superplasticizer to the combined mass of cement and soil. Referred to as the polycarboxylate superplasticizer content (*P*).
3. The ratio of the mass of water to the total mass of solid particles. Referred to as the water-to-solid ratio (*W*).

A CLSM sample is denoted as C10W34P0.1, where C is 10%, W is 34%, and P is 0.1%. To ensure

economic and environmental benefits, the cement content in CLSM is generally limited to below 25% (CSWADI, 2022), while *W* is set higher than the soil's liquid limit to achieve adequate flowability. Based on preliminary small-scale tests, the mix proportions for samples without polycarboxylate superplasticizer are listed as IDs1-16 in Table 2. These proportions were used to evaluate the feasibility of producing CLSM with red-bed mudstone, cement, and water. To investigate the effect of polycarboxylate superplasticizer dosage on CLSM performance, *P* levels were set at 0%, 0.1%, 0.2%, 0.3%, and 0.4%, in accordance with the Chinese Standard DBJ51/T 188-2022. The corresponding values of *C* and *W* are provided as IDs17-27 in Table 2.

Table 2 Mix proportions for soil-based CLSM mixes.

ID	*C* (%)	*W* (%)	Dry red-bed mudstone (kg/m^3)	Cement (kg/m^3)	Water (kg/m^3)
1	4	44	1189	48	576
2	4	48	1133	45	598
3	4	52	1082	43	619
4	4	56	1036	41	638
5	8	44	1148	92	555
6	8	48	1093	87	577
7	8	52	1044	84	597
8	8	56	999	80	615
9	12	44	1109	133	537
10	12	48	1056	127	558
11	12	52	1009	121	577
12	12	56	965	116	594
13	16	44	1073	172	519
14	16	48	1022	163	539
15	16	52	975	156	558
16	16	56	933	149	575
17	10	34	1395	139	522
18	10	36	1356	136	537
19	10	38	1320	132	552
20	10	40	1286	129	556
21	10	43	1238	124	585
22	10	46	1193	119	604
23	10	49	1151	115	621
24	10	52	1113	111	636
25	10	55	1076	108	651
26	10	58	1042	104	665

27	10	61	1010	101	678

2.3 Test methods

2.3.1 Types of tests

The experimental procedure is illustrated in Fig. 5. Cement, polycarboxylate superplasticizer, and water were initially blended in a mortar mixer for 60 s. Red-bed mudstone was then added, and the mixture was stirred for an additional 180 s. After mixing, the CLSM was tested for flowability, bleeding rate, setting time and settlement rate. A portion of the mixture was poured into moulds, labelled and cured in a standard curing room at 20±2°C with approximately 95% relative humidity. Following the designated curing period, the samples were tested for compressive strength, drying shrinkage rate, and water stability.

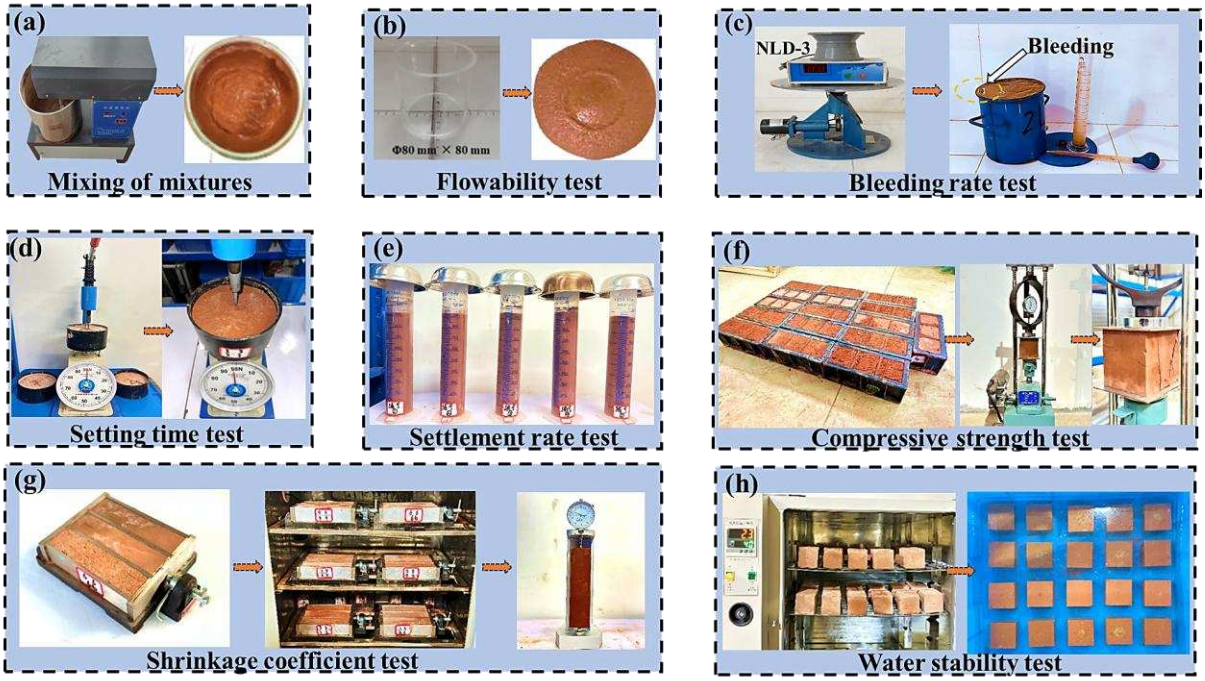

Fig. 5. Flowchart of the experimental procedure.

2.3.2 Testing of Fresh mix Properties

(1) Flowability test

Flowability is a key design parameter for CLSM, with higher flowability facilitating self-

compaction during construction. Following the Japan standard JHS A313-1992, a cylindrical container (80 mm in diameter and height) was filled with fresh CLSM mixtures and lifted slowly over 5 seconds to allow the material to spread freely. Once the flow ceased, the diameters in two perpendicular directions were measured, and the average was recorded as the flowability of the CLSM. For applications where on-site mixing is limited, the effect of cement hydration on flowability during transportation was evaluated. CLSM flowability was measured at intervals of 0, 15, 30, 60, 90, 120, and 180 min after mixing.

(2) Bleeding rate test

After pouring, solid particles in CLSM settle under gravity, resulting in surface bleeding. The bleeding rate (*Br*)) should generally remain below 5% (Qian et al., 2015). According to the Chinese Standard JTG 3420-2020, *Br* is measured using a cylindrical container with a diameter of 137 mm and a height of 138 mm. Freshly mixed CLSM is placed into the container, vibrated 120 times using a flowability tester, and left to stand with a lid. During the first hour, surface bleeding water is collected every 10 min, and subsequently every 30 min until bleeding stops. The bleeding rate is calculated as the ratio of the total mass of extracted water to the initial water content in the CLSM mixture.

(3) Setting time test

The setting time (T_s) is a critical parameter for planning CLSM construction (Chittoori et al., 2014). According to the Chinese Standard JGJ/T70-2009, T_s is determined using a ZKS-100 setting time tester. The CLSM mixture is placed in a container and left to stand for 2 hours before testing begins, with measurements taken every 30 min. During each test, a needle with a cross-sectional area (*Ap*) of 30 mm² is inserted 25 mm into the CLSM, and the static pressure (N_p) is recorded. The penetration resistance (f_p) is calculated using Eq. (1), which relates static pressure to the needle area.

When (f_p) reaches 0.3 MPa, measurements are taken every 15 min until (f_p) reaches 0.7 MPa. The time corresponding to f_p=0.5 MPa, derived from the plotted curve of (f_p) versus time, is defined as T_s.

$$f_p = \frac{N_p}{A_p} \tag{1}$$

2.3.3 Testing of hardened mix properties

(1) Settlement rate test

The sedimentation of solid particles and cement hydration following CLSM mixing can contribute to increased settlement. To assess this, the settlement rate (h_{sr}) of CLSM was measured (Paul et al., 2004). The CLSM mixture was placed in a cylindrical container with a capacity of 1000 ml and marked sidewalls. The container was sealed with plastic film and a lid. The height of the mixture was periodically recorded, and h_{sr} was calculated using Eq. (2).

$$h_{sr} = \frac{h_0 - h_s}{h_0} \tag{2}$$

Where, h_s (%) is the Settlement rate; h_0 (mm) is the initial height of mixture; and h (mm) is the stable settlement height of mixture.

(2) Compressive strength test

The CLSM was mixed and poured into cubic moulds with a side length of 70.7 mm, then cured in a standard curing room. Compressive strength (q_u) tests were conducted over 28 days in accordance with the Chinese standard JGJ/T 233-2011, using an unconfined compressive strength tester designed for lime-soil.

2.3.4 Testing of hardened mix Durability

(1) Shrinkage coefficient test

The high water content in CLSM can lead to drying shrinkage and cracking (ACI, 1999; Qian et

al., 2019). To study this, the drying shrinkage rate was tested following the Chinese standard JGJ/T70-2009. Freshly mixed CLSM was poured into prismatic moulds (40 mm×40 mm×160 mm). After 7 days of curing, the initial length L_0 of the specimens was measured in a standard curing room. The specimens were then transferred to a curing environment, maintained at (20±2)℃ and (60±5) relative humidity. Length measurements were taken on days 14, 21, 28, and 56, and the drying shrinkage rate was calculated using Eq. (3). Specimen mass was also recorded during each measurement to determine the water loss rate, providing supplementary data for analysing drying shrinkage.

$$\varepsilon_{at} = \frac{L_0 - L_t}{L - L_d} \tag{3}$$

Where, ε_{at} (%) is the drying shrinkage rate; L_0(mm) is the length of specimen after curing for 7 d; L (160 mm) is the length of moulds; L_d (20±2 mm) is the length of the shrink screw inserted into the mixture; L_t (mm) is the length of specimen after curing for t d.

(2) Water stability test

The poor water stability of red-bed mudstone may result in insufficient water stability in the prepared CLSM. To evaluate this, a dry-wet cycling test was conducted based on cement-based material testing methods (Ahmed and Ugai, 2011; Khattab et al., 2007). Specimens cured for 28 d were dried in a 65 ℃ electric oven for 48 hours and then immersed in 20℃ water for 24 hours to complete one dry-wet cycle. Compressive strength was tested after 1, 3, 5, 7, 9, and 11 cycles. For each mixture, specimens were divided into two groups. One group was cured for 27 d, soaked in water for 24 hours, and tested for compressive strength (q_{u0}). The other group underwent N dry-wet cycles before testing, with the compressive strength recorded as q_{un}. The residual strength (r_q) was calculated using Eq. (4) to assess the water stability of CLSM.

$$r_q = \frac{q_{un} - q_{u0}}{q_{u0}} \quad (4)$$

3. Results and Discussion

Based on the experimental methods and mix designs described earlier, this section presents and discusses the results of using waste red-bed mudstone in CLSM production. The effects of varying cement-to-soil ratios (C), water-to-solid ratios (W), and polycarboxylate superplasticizer dosages (P) on the fresh, hardened, and durability properties of the CLSM mixtures are analyzed. This aims to optimize the mix formulations to achieve desirable performance characteristics for sustainable backfill applications.

3.1 Properties of the fresh mix

3.1.1 Flowability

(1) Initial flowability

The flowability of CLSM immediately after mixing is defined as the initial flowability (f_0). When the quantity of polycarboxylate superplasticizer (P=0) is 0, the test results for f_0 are shown in Fig. 6. Except for the sample with a water-to-solid ratio (W) of 44%, all other samples achieved (f_0) values exceeding 180 mm, meeting the self-compaction requirements for backfilling in narrow spaces such as behind bridge abutments, culverts, and retaining walls (ACI, 1999). For other backfilling applications, f_0 should be adjusted based on the working area size and the availability of vibration compaction. As illustrated in Fig. 6, f_0 increases with higher W and cement-to-soil ratio (C) (Du et al., 2024; Wang, 1997; Huang et al., 2021). Water in the sample exists as bound water on particle surfaces and free water between particles, with flowability primarily determined by the free water content. When C is constant and W increases, the free water content rises, increasing particle spacing and

reducing cohesive and frictional forces, thereby improving flowability. Additionally, during cement hydration, free Ca^{2+} ions react with Na^{+} and K^{+} ions on soil particle surfaces, reducing the thickness of the electric double layer. This reaction thins the bound water layer on particle surfaces, increases free water content, and further enhances flowability. Consequently, increasing C also improves the flowability of the sample (Du et al., 2024).

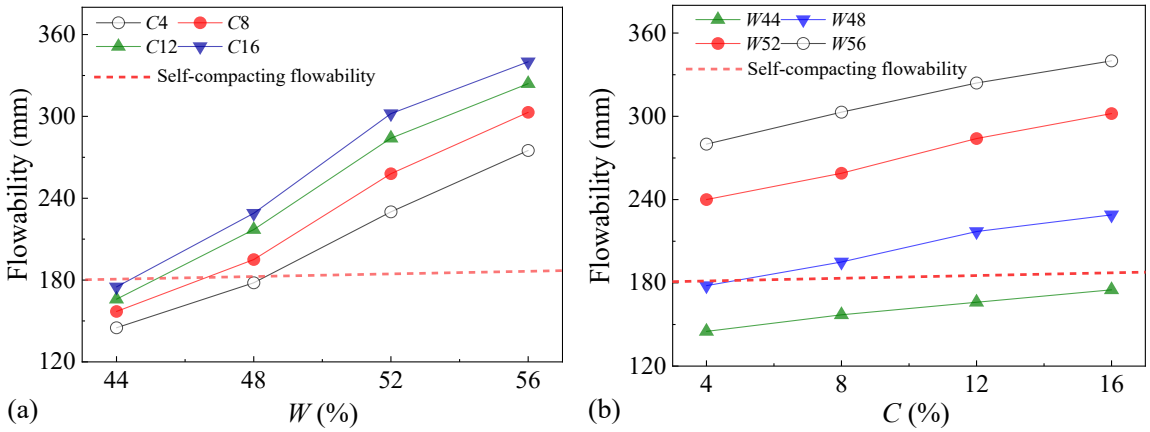

Fig. 6. Initial flowability variations of samples without superplasticizer (P = 0): (a) effect of C; (b) effect of W.

To quantitatively analyse the effect of W on flowability, a normalization factor $X_f(W)$ for f_0 was introduced (Chang et al., 2015), as defined in Eq. (5). The calculation results are shown in Fig. 7(a), from which the fitted functional relationship between $X_f(W)$ and W is derived in Eq. (7). Similarly, a normalization factor $X_f(C)$ for f_0 and C was introduced based on Fig. 6(b), as defined in Eq. (6). The fitted relationship between $X_f(C)$ and C is provided in Eq. (8).

$$X_f(W) = \frac{f_0(C,W) - f_0(C,44)}{f_0(C,56) - f_0(C,44)} \tag{5}$$

$$X_f(C) = \frac{f_0(C,W) - f_0(4,W)}{f_0(16,W) - f_0(4,W)} \tag{6}$$

where, $f_0(16,W)$, $f_0(4,W)$ represent initial flowability at C values of 16% and 4%, respectively. $f_0(C,56)$,$f_0(C,44)$ represent initial flowability at W values of 56% and 44%, respectively.

By simultaneously solving Eq. (5) and Eq. (6) and substituting the key data points $f_0(16,56)$, $f_0(16,44)$, $f_0(4,56)$ and $f_0(4,44)$, the expression for f_0 as a function of C and W is derived, as shown in

Eq. (9). Fig. 8 demonstrates that the regression formula aligns well with the experimental data within the ranges of W from 44% to 56% and C from 4% to 16%.

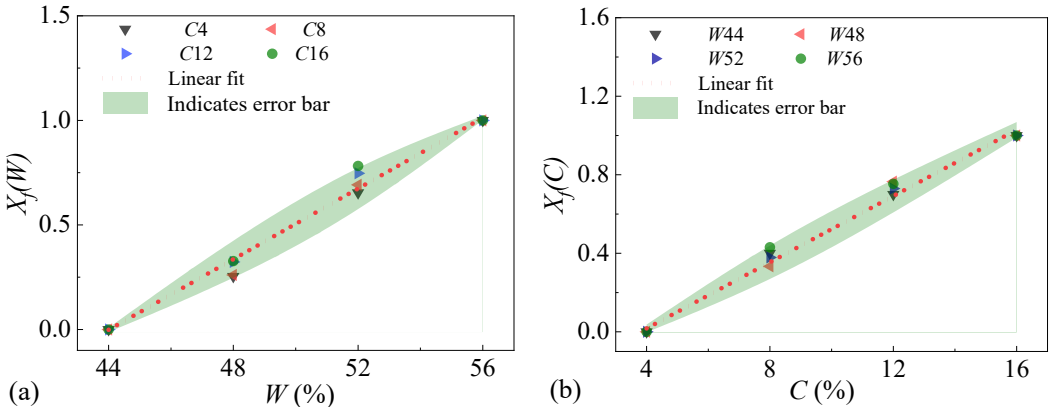

Fig. 7. Fitted functions for flowability factors: (a) $X_f(W)$ versus W; (b) $X_f(C)$ versus C.

$$X_f(W) = 8.45W - 3.72 \tag{7}$$

$$X_f(C) = 8.43C - 0.32 \tag{8}$$

$$f_0(C,W) = 2493CW + 1004W - 845C - 307 \tag{9}$$

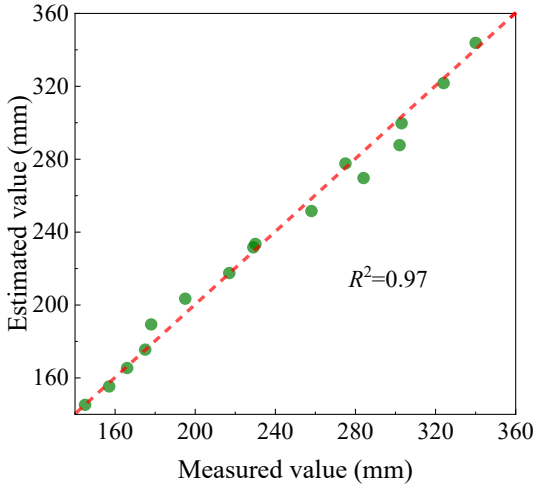

Fig. 8. Comparison between measured and predicted flowability values.

The initial flowability (f_0) of samples supplemented with polycarboxylate superplasticizer is shown in Fig. 9. The results indicate that with fixed C and W, f_0 increases as the quantity of polycarboxylate superplasticizer (P) increases. During mixing, cement and soil particles tend to aggregate due to van der Waals forces, trapping free water within solid clusters. This reduces the mobility of free water and lowers the sample's flowability. When polycarboxylate superplasticizer is

added, its anionic groups anchor onto particle surfaces, creating electrostatic repulsion, while its side chains provide steric hindrance when particle spacing is small, as illustrated in Fig. 10 (Hu et al., 2024; Wang et al., 2024). These repulsive forces, comprising steric hindrance and electrostatic repulsion, overcome van der Waals forces, dispersing the aggregated particles and releasing trapped free water, thereby increasing the flowability of the sample.

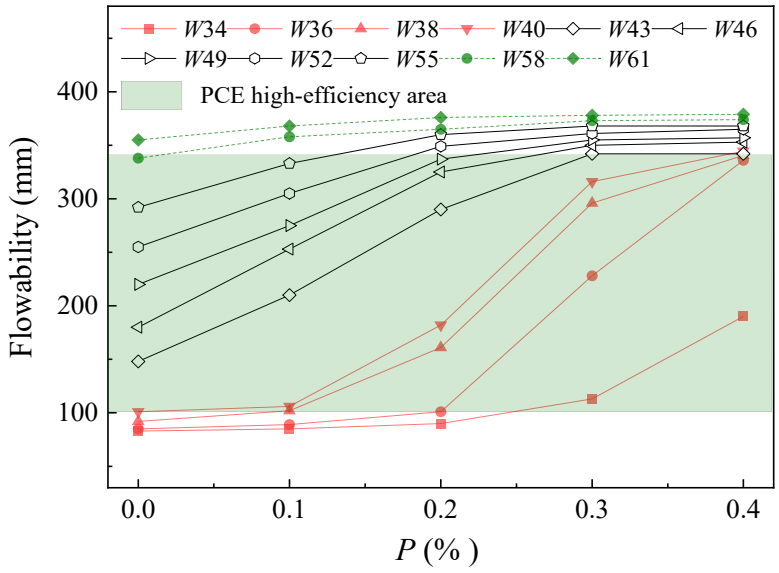

Fig. 9. Initial flowability variations of samples with polycarboxylate superplasticizer volume (P) at fixed C = 10%.

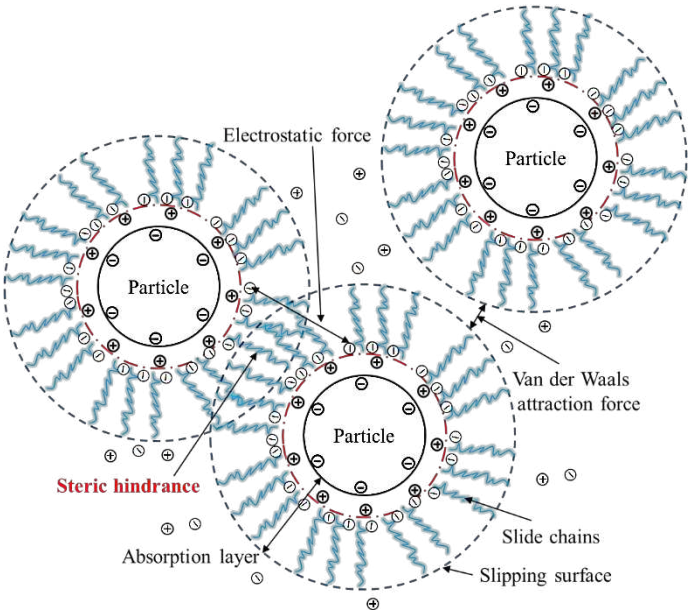

Fig. 10. Conceptual illustration of adsorption and repulsion between solid particles and polycarboxylate superplasticizer. Modified from Zhang et al.(2023)

Fig. 9 illustrates that at low W values (flowability below 100 mm), P must exceed a critical threshold to significantly improve flowability. For instance, when W = 34%, P must reach 0.30%, while for W values of 36% and 40%, the critical thresholds are 0.20% and 0.10%, respectively. This suggests that when W is low, the initial water content in the sample is insufficient, leading to significant interparticle friction and cohesion. Additionally, the low water content restricts the amount of free water released from agglomerated particles. As a result, the addition of the polycarboxylate superplasticizer has minimal improvement in flowability. At W = 58% (flowability of 340 mm), the influence of P on flowability diminishes. At higher W, sufficient free water is already present between particles, and the flowability reaches its maximum, with the sample nearing segregation (Hu et al., 2024; He et al., 2020). Further increases in P lead to water bleeding, causing segregation, as shown in Fig. 11. For CLSM prepared with the red-bed mudstone used in this study, it is recommended to apply polycarboxylate superplasticizers within a W range of 43%-58%.

Fig. 11. Segregation observed in specimen $C10W58P0.2$.

To assess the impact of polycarboxylate superplasticizer on the water content of the mixture at the same flowability design standard (f_a), the water reduction rate of the polycarboxylate superplasticizer is defined, as shown in Eq. (10).

$$W_R = \frac{W_0 - W_P}{W_0} \tag{10}$$

where, W_R (%) is the water reduction rate of the polycarboxylate superplasticizer; W_0 (kg.m^{-3}) is the unit water content of the sample without polycarboxylate superplasticizer at flowability design standard (f_a), and W_p (kg.m^{-3}) is the unit water content of the sample with polycarboxylate superplasticizer at f_a.

When the initial flowability (f_0) deviates from the flowability design standard (f_a) by less than 5 mm, it is considered to meet engineering requirements. For example, if f_a = 85 mm, acceptable f_0 values range from 80 mm to 90 mm. Selected W_R values for the samples are shown in Table 3. For f_a below 100 mm, W_R is approximately 0 when P = 0.2%. For f_a between 165 mm and 285 mm, W_R ranges from 8.62% to 10.17% at P = 0.2%. However, when f_a increases to 335 mm, W_R decreases to 6.69% at the same P. These results indicate that polycarboxylate superplasticizer are most effective when the flowability design standard for backfilling projects lies between 165 mm and 285 mm.

Table 3 Water reduction rates (W_R %) achieved by polycarboxylate superplasticizer.

ID	f_0 (mm)	f_a (mm)	Water (kg/m^{-3})	W_R (%)
*C*10*W*34	83	85	482	0.21
*C*10*W*34*P*0.2	90		481	
*C*10*W*36	92	95	496	0.20
*C*10*W*36*P*0.2	100		495	
*C*10*W*46	170	165	170	8.62
*C*10*W*38*P*0.2	161		161	
*C*10*W*55	290	285	290	10.17
*C*10*W*43*P*0.2	290		290	
*C*10*W*58	338	335	338	6.69
*C*10*W*49*P*0.2	337		337	

(2) Time-dependent flowability

The flowability measured after a specific time (t) is referred to as time-dependent flowability $f(t)$.

Fig. 12(a) presents the flowability of samples without polycarboxylate superplasticizer, demonstrating that $f(t)$ decreases over time, with the rate of decline gradually slowing. Although the initial flowability (f_0) of the $W48C12$ sample meets self-compaction requirements, its flowability falls below the standard after 60 min. This underscores the importance of considering the time-dependent loss of CLSM flowability in practical applications. Fig. 12(b) shows the flowability of samples with polycarboxylate superplasticizer. The variation in $f(t)$ over time follows a similar trend to that of samples without polycarboxylate superplasticizer.

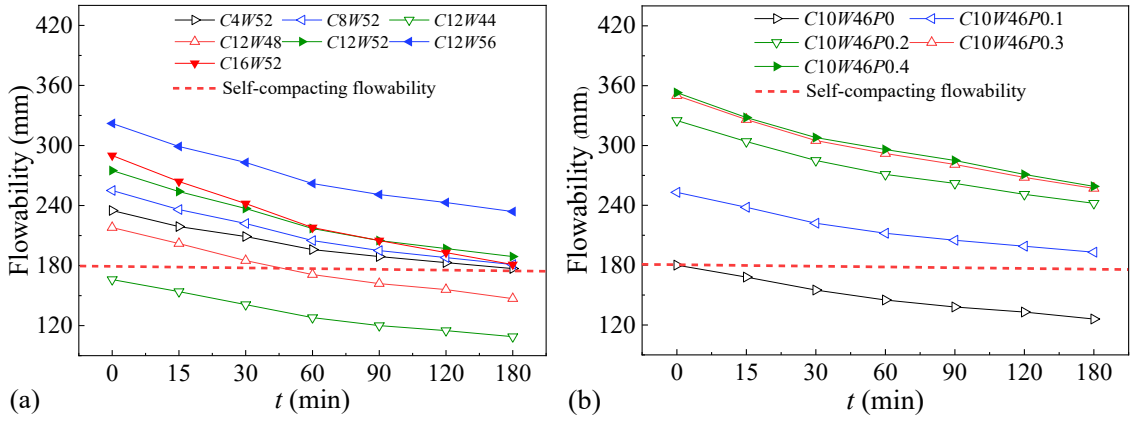

Fig. 12. Time-dependent changes in flowability: (a) samples without polycarboxylate superplasticizer; (b) samples with polycarboxylate superplasticizer.

In this study, the flowability loss rate $r_f(t)$ was introduced to quantitatively describe the relationship between $f(t)$ and time t, as defined in Eq. (11). For samples without polycarboxylate superplasticizer, $r_f(t)$ exhibits a logarithmic relationship with t, as shown in Fig. 13(a). At 180 minutes, the mean $r_f(t)$ is approximately 30%. Notably, the relationship between $r_f(t)$ and t is affected by W and C. At a constant W, $r_f(t)$ increases with C. For instance, at 180 min, $r_f(t)$ is 26% for $W52C4$ while $r_f(t)$ is 35% for $W52C16$, likely due to accelerated setting caused by the higher C. Conversely, considering C = 12%, increasing W from 44% to 56% reduces $r_f(t)$ from 34% to 27%. This reduction is attributed to the higher water content delaying the formation of a cohesive skeleton from cement hydration

products, thereby mitigating flowability loss (Huang, 2000). For samples with polycarboxylate superplasticizer, $r_f(t)$ also follows a logarithmic function of t, as shown in Fig. 13(b). The $r_f(t)$ is approximately 26% at 180 min. At constant C and W, increasing P reduces $r_f(t)$. For example, at 180 min, the $r_f(t)$ of samples with P = 0 and P = 0.40% differs by approximately 10%, attributed to the higher polycarboxylate superplasticizer content increasing free water between particles (Deng et al., 2011; Huang, 2000).

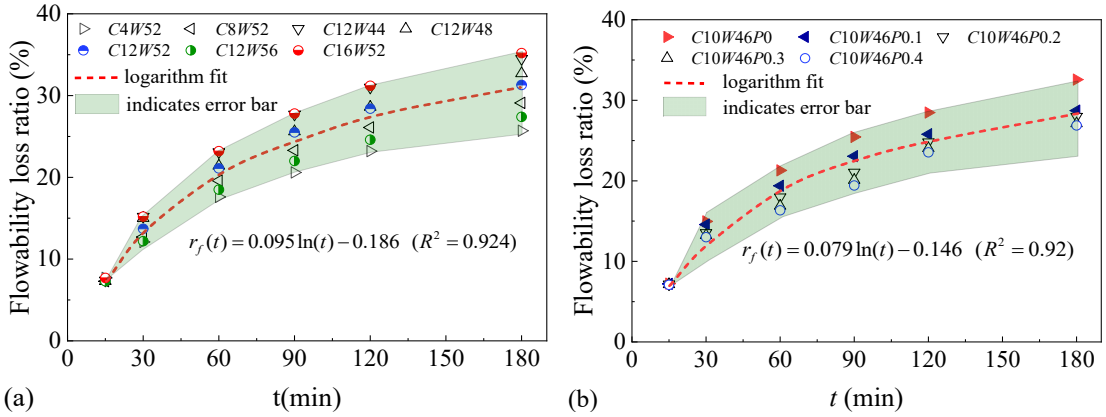

Fig. 13. Time-dependent flowability loss ratios: (a) samples without polycarboxylate superplasticizer; (b) samples with polycarboxylate superplasticizer.

$$r_f(t) = [f_0 - f(t)] / f_0 \quad (11)$$

3.1.2 Bleeding Rate

For samples without polycarboxylate superplasticizer, the bleeding rate (B_r) is shown in Fig. 14 (a). B_r increases rapidly within the first 90 min and then stabilizes. Fig. 14 (a) also illustrates that, at a constant W, C has minimal impact on B_r. However, when C = 12% and W increases from 44% to 56%, B_r rises from 0.5% to 4.9%, approaching the maximum permissible B_r for engineering applications. For samples with polycarboxylate superplasticizer, (B_r) is presented in Fig. 14 (b). At constant C and W, increasing the polycarboxylate superplasticizer dosage significantly raises B_r. This is because the polycarboxylate superplasticizer disperses aggregated particles, facilitating their sedimentation and releasing trapped free water. For example, the B_r of sample W46C10P0.4 exceeds 5%, failing to meet

design standards (Qian et al., 2015). Notably, when assessing the impact of the polycarboxylate superplasticizer on B_r under the same flowability design standard (f_a), the results differ. According to the flowability test data in Figs. 6 and 9, both the $C12W52$ and $C10W46P0.1$ samples exhibit a flowability of approximately 255 mm. However, Fig. 14 shows that their B_r values are 3.55% and 1.78%, respectively. This demonstrates that, at the same flowability, adding polycarboxylate superplasticizer reduces W, thereby decreasing B_r.

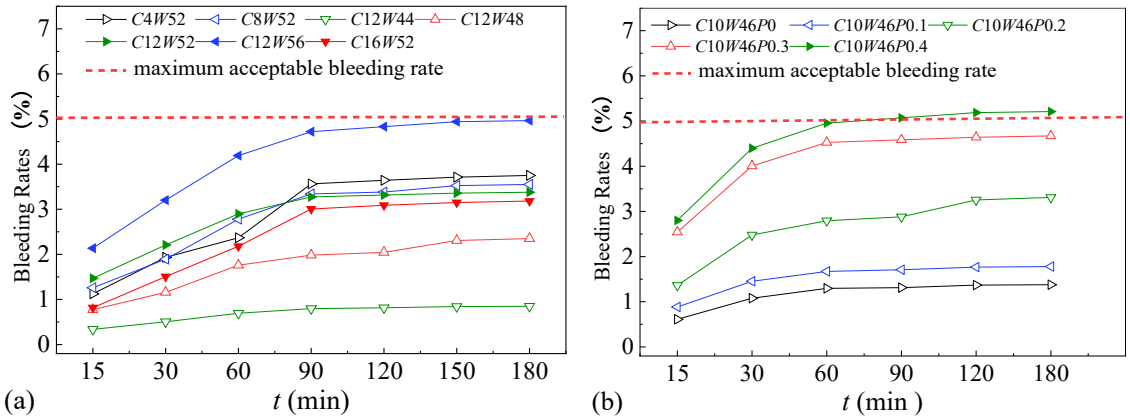

Fig. 14. Time-dependent changes in bleeding rates: (a) samples without polycarboxylate superplasticizer; (b) samples with polycarboxylate superplasticizer.

3.1.3 Setting Time

The setting time (T_s) test results are summarized in Table 4. Without polycarboxylate superplasticizer, T_s increased by approximately 2 hours when C = 12% and W rose from 44% to 48%, as the higher water content significantly delayed the formation of a cohesive skeleton through cement hydration (Du et al., 2024; Qian et al., 2015). Conversely, when W = 52% and C increased from 4% to 16%, T_s decreased from 19 hours to 9 hours. All samples had T_s values within 24 hours, meeting construction time requirements (Chittoori et al., 2014). After adding the polycarboxylate superplasticizer, T_s increases with the rise in P when C and W remain constant, indicating a measurable retarding effect of the polycarboxylate superplasticizer. Moreover, the $C12W52$ and $C10W46P0.1$

samples exhibit the same flowability and only minor differences in T_s, suggesting that under identical flowability design standards, the retarding effect of the polycarboxylate superplasticizer on T_s diminishes.

Table 4. Setting times (T_s) of samples under various mix proportions.

ID	*C*4*W*52	*C*8*W*52	*C*12*W*44	*C*12*W*48	*C*12*W*52	*C*12*W*56	*C*16*W*52
T_s (h)	19.0	16.0	8.5	10.5	15.0	15.5	9.0
ID	*C*10*W*46*P*0		*C*10*W*46*P*0.1	*C*10*W*46*P*0.2	*C*10*W*46*P*0.3		*C*10*W*46*P*0.4
T_s (h)	14.0		14.5	17.5	19.5		22.0

3.2 Properties of the hardened mix

3.3.1 Settlement rate

For samples without polycarboxylate superplasticizer, the settlement rate (h_r) is presented in Table 5. h_r increases rapidly during the first 12 hours and stabilizes by the second day. When C = 12% and W rises from 44% to 56%, the 9 d h_r increases from 0.5% to 4.5%, approaching the engineering limit of 5%. Thus, W should be maintained below 56%. The settlement behaviour is illustrated in Fig. 15, where the settlement of the mixture (h_0–h_s) exceeds the bleeding height (h_w–h_s). Additionally, Table 5 shows that at a fixed W, h_r increases with higher C. This indicates that h_r in CLSM is influenced not only by bleeding but also by other factors, such as chemical shrinkage during cement hydration and air expulsion (Zhang et al., 2010).

Table 5 Settlement rate (h_r /%) of samples without polycarboxylate superplasticizer.

ID	1h	4h	12h	1 d	2 d	3 d	4 d	5 d	6 d	7 d	8 d	9 d
*C*4*W*52	0.5	1.0	1.5	0.2	2.5	2.5	2.5	2.5	2.5	2.5	2.5	2.5
*C*8*W*52	0.5	1.5	2.0	2.5	3.0	3.0	3.0	3.0	3.0	3.0	3.0	3.0
*C*12*W*44	0.0	0.0	0.5	0.5	0.5	0.5	0.5	0.5	0.5	0.5	0.5	0.5
*C*12*W*48	0.0	0.5	1.0	1.5	1.5	1.5	1.5	1.5	1.5	1.5	1.5	1.5
*C*12*W*52	0.5	1.5	2.0	2.5	3.0	3.0	3.0	3.0	3.0	3.0	3.0	3.0

*C*12*W*56	1.0	2.5	3.5	4.0	4.5	4.5	4.5	4.5	4.5	4.5	4.5	4.5
*C*16*W*52	1.0	2.0	3.0	3.5	3.5	3.5	3.5	3.5	3.5	3.5	3.5	3.5

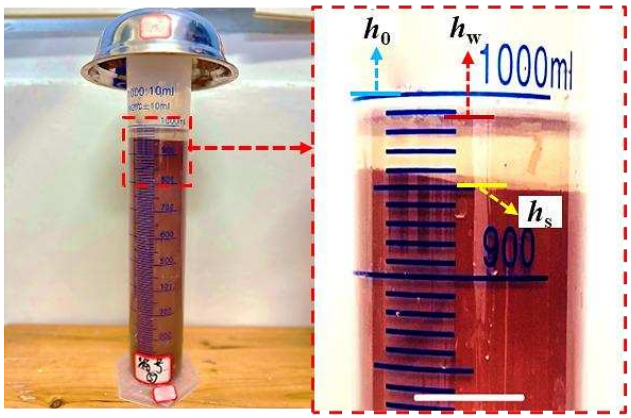

Fig. 15. Settlement condition of sample *C*12*W*56 after 3 d.

The settlement rate (h_r) test results for samples with polycarboxylate superplasticizer are shown in Table 6. (h_r) stabilizes after 3 d, consistent with the behaviour of samples without polycarboxylate superplasticizer. When C = 10% and W = 46%, adding 0.4% polycarboxylate superplasticizer increases the settlement rate to 6.0%, exceeding the typical engineering limit (Paul et al., 2004). This is primarily due to the polycarboxylate superplasticizer promoting particle sedimentation and bleeding, leading to increased settlement (Paul et al., 2004). However, At the same flowability (255 mm), the settlement rates of *C*10*W*46*P*0.1 and *C*12*W*52 are approximately 2% and 3%, respectively. This comparison indicates that adding 0.1% polycarboxylate superplasticizer reduces the settlement rate by 1%.

Table 6. Settlement rate (h_r /%) of samples with polycarboxylate superplasticizer.

ID	1 h	4 h	12 h	1 d	2 d	3 d	4 d	5 d	6 d	7 d	8 d	9 d
*C*10*W*46*P*0	0.5	1.0	1.5	1.5	2.0	2.0	2.0	2.0	2.0	2.0	2.0	2.0
*C*10*W*46*P*0.1	0.5	1.0	1.5	1.5	2.0	2.0	2.0	2.0	2.0	2.0	2.0	2.0
*C*10*W*46*P*0.2	0.5	1.0	2.0	2.5	3.0	3.0	3.0	3.0	3.0	3.0	3.0	3.0
*C*10*W*46*P*0.3	0.5	1.0	2.0	3.0	4.0	4.5	4.5	4.5	4.5	4.5	4.5	4.5
*C*10*W*46*P*0.4	1.0	2.0	3.0	4.0	5.0	6.0	6.0	6.0	6.0	6.0	6.0	6.0

3.3.2 Compressive Strength

The compressive strength (q_u) test results are presented in Fig. 16. At a constant C, q_u decreases linearly as W increases. Conversely, at a constant W, q_u increases linearly with higher C.

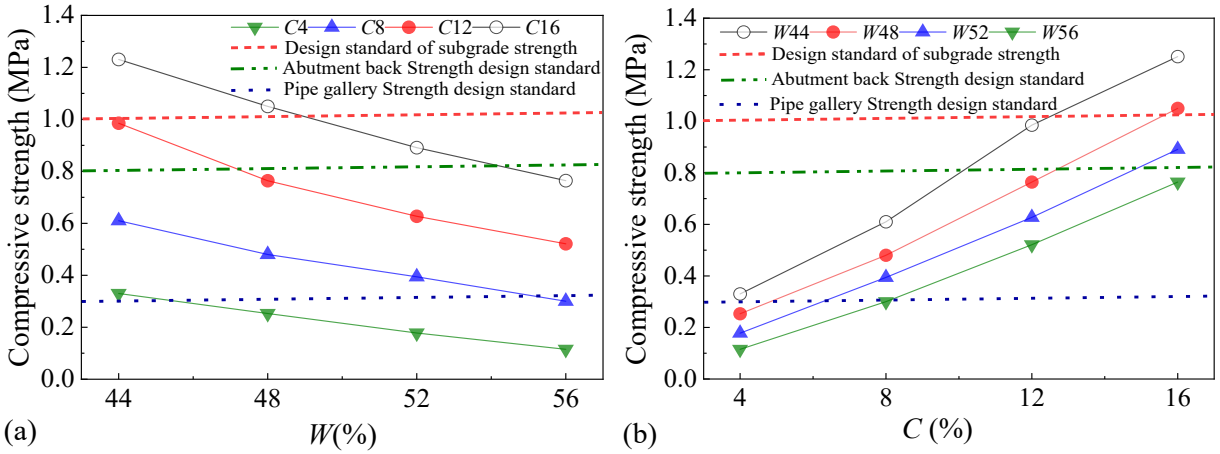

Fig. 16. Variations in compressive strength of samples without superplasticizer (P = 0): (a) effect of W; (b) effect of C.

An increase in C enhances q_u, primarily due to hydration reactions between cement minerals (e.g., tetracalcium aluminoferrite) and water, resulting in the formation of Calcium Silicate Hydrate (C-S-H), $Ca(OH)_2$, and needle-shaped Ettringite (Aft), as shown in Fig. 17. Following this, $Ca(OH)_2$ reacts with SiO_2 and other active components in the red-bed mudstone via pozzolanic reactions, further generating C-S-H. These hydration products, such as C-S-H and ettringite, interweave to form a network structure that encapsulates soil particles, creating a skeleton that improves strength (Du et al., 2024; Huang et al., 2006). To further investigate the hydration products and strength development mechanism, energy-dispersive spectroscopy (EDS) was performed on the needle-like structure in Fig. 17(a) and the network skeleton in Fig. 17(b). Based on the chemical formula of Ettringite ($3CaO{\cdot}Al_2O3{\cdot}3CaSO_4{\cdot}32H_2O$), its primary elements are Ca, O, Al, and H (note H is undetectable via EDS). The EDS mapping in Fig. 18(a) further suggests that the needle-shaped structure is Ettringite (Huang, 2000). Fig. 18(b) indicates that the network skeleton contains Ca, O, Si, Al, and Fe. According

to the chemical formula of C-S-H ($Ca_5Si_6O_{16}(OH)\cdot 4H_2O$), its main elements are Ca, O, Si, and Al, with Fe originating from hydration products of Tetracalcium Aluminoferrite. Therefore, the network skeleton likely forms from the interweaving of C-S-H, ettringite, and other hydration products.

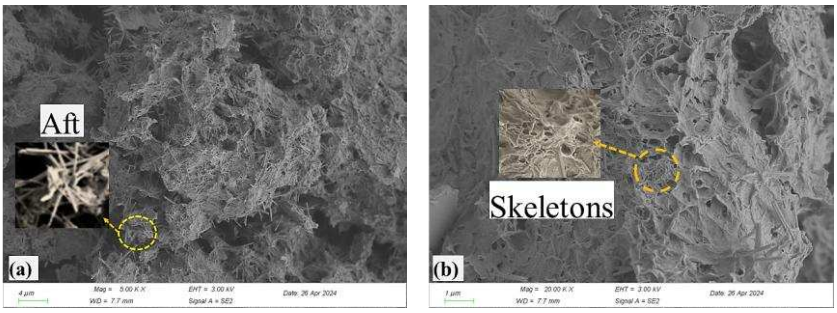

Fig. 17. Scanning electron microscopy (SEM) images of sample *C*8*W*52: (a) needle-like structures; (b) reticular skeletons.

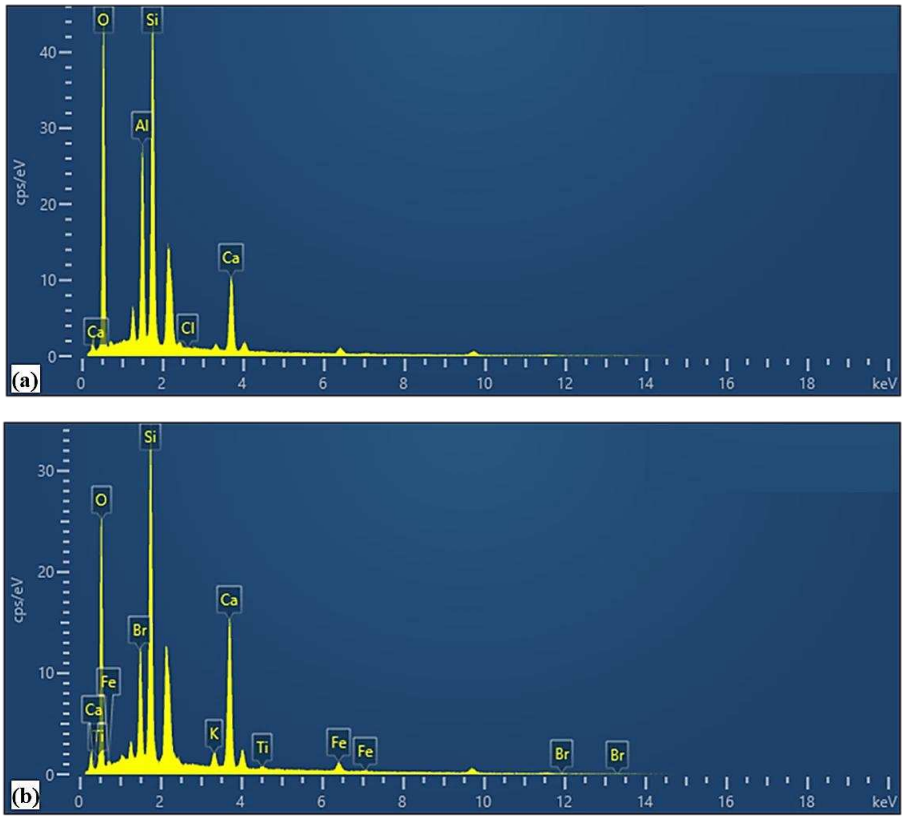

Fig. 18. EDS spectra of hydration products in samples: (a) needle-like structures; (b) reticular skeletons.

The variation of q_u demonstrates a clear relationship with C and W. Using a method similar to that for deriving the initial flowability (f_0), normalization factors $X_q(C)$ and $X_q(W)$ were introduced to establish an expression for q_u as a function of C and W. The estimation accuracy was validated within

464 the ranges of C = 4%-16% and W = 44%-56%, and the final form is presented in Eq. (14). The 28-day
465 q_u requirements depend on the application scenario: for non-load-bearing narrow spaces such as
466 foundation trenches, q_u should be at least 0.3 MPa; for transportation engineering applications (bridge
467 abutments, culvert backs, and retaining walls), q_u should be at least 0.8 MPa; and for general subgrade
468 or temporary roads, q_u should be at least 1 MPa (CSWADI, 2022). Experimental results indicate that,
469 except for samples with C = 4%, CLSM with C = 8%-16% and W = 44%-56% achieves q_u values
470 ranging from 0.3 MPa to 1.3 MPa, meeting the requirements for a variety of engineering applications.

471 $$q_u(C,W) = -17.54CW + 15.20C - 1.04W + 0.46 \quad (R^2 = 0.978) \qquad (12)$$

472 The 28-day compressive strength (q_u) of samples with polycarboxylate superplasticizer is shown
473 in Fig. 19. The relationship between q_u and polycarboxylate superplasticizer dosage P does not follow
474 a consistent trend. When C = 10% and W = 43%, q_u increases continuously as P rises. The addition of
475 the polycarboxylate superplasticizer promotes particle dispersion, leading to uniformly dense packing
476 (Yu et al., 2017). Furthermore, adding an appropriate amount of polycarboxylate superplasticizer
477 enhances the production of ultimate cement hydration products. (Chen et al., 2015). In contrast, when
478 C = 10% and W = 46%, q_u begins to decrease when P is 0.4%. For samples with C = 10% and W =
479 61%, q_u decreases immediately upon the addition of polycarboxylate superplasticizer. Table 7
480 summarizes the flowability and bleeding rates of samples where q_u decreases. These samples exhibit
481 initial flowability values above 340 mm and bleeding rates exceeding 5%. This suggests that excessive
482 polycarboxylate superplasticizer causes significant bleeding, leading to the formation of a weak
483 surface layer and a consequent reduction in q_u (He et al., 2020; Yu et al., 2017).

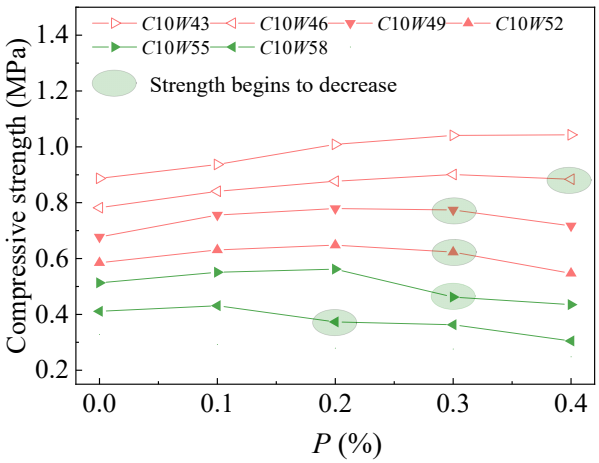

Fig. 19. Relationship between compressive strength and P of samples.

Table 7 Initial flowability (f_0) and bleeding rates (B_r) of samples where compressive strength begins to decrease.

ID	*C*10*W*46*P*0.4	*C*10*W*49*P*0.3	*C*10*W*52*P*0.3	*C*10*W*55*P*0.3	*C*10*W*58*P*0.2
f_0 (mm)	353	355	361	368	365
B_r (%)	5.11	5.48	6.39	7.53	7.79

The compressive strength (q_u) of samples with and without polycarboxylate superplasticizer at the same flowability design standard (f_a) is summarized in Table 8. At f_a = 215 mm, comparing *C*10*W*43*P*0.1 and *C*10*W*49, the addition of 0.1% polycarboxylate superplasticizer reduces W by 6% and increases q_u by 0.284 MPa. Similarly, at f_a = 250 mm, comparing *C*10*W*46*P*0.1 and *C*10*W*52, the same polycarboxylate superplasticizer dosage reduces W by 6% and increases q_u by 0.256 MPa. The polycarboxylate superplasticizer lowers the W needed to achieve the flowability standard, which in turn reduces the C required to meet the compressive strength standard. The addition of the polycarboxylate superplasticizer helps address the challenges of high water and cement content in CLSM, mitigating the negative effects of excessive water on hardened performance. Furthermore, it reduces cement costs and decreases carbon emissions associated with cement production (Carrasco et al., 2019).

Table 8 Compressive strength of samples under the same flowability design standard (f_a).

ID	f_0 (mm)	f_a (mm)	q_u (MPa)

*C*10*W*49	220	215	0.677
*C*10*W*43*P*0.1	210		0.961
*C*10*W*52	255	250	0.585
*C*10*W*46*P*0.1	253		0.841
*C*10*W*55	290	290	0.513
*C*10*W*43*P*0.2	290		1.008
*C*10*W*58	338	335	0.411
*C*10*W*55*P*0.1	333		0.551
*C*10*W*49*P*0.2	337		0.779

3.3 CLSM Durability

3.3.1 Drying shrinkage rate

The drying shrinkage rate (ε_{at}) test results for samples without polycarboxylate superplasticizer are summarised in Table 8, with temporal trends illustrated in Fig. 20(a). The water loss rate (w_r) results are presented in Fig. 20(b). As shown in Table 8, all samples except C4W52 maintain ε_{at} below 1.5%, with no cracking observed. At a constant water-to-solid ratio (W), the influence of the cement-to-soil ratio (C) on ε_{at} varies over time. At 14 d, ε_{at} increases with higher C, primarily due to strong cement hydration reactions during this period, resulting in significant chemical shrinkage (Di Bella et al., 2017). However, between 14 and 56 d, ε_{at} decreases as C increases. This is attributed to reduced hydration activity after 14 d, which weakens chemical shrinkage. Furthermore, hydration products, including C-S-H and ettringite, occupy the voids between soil particles, enhancing the sample's ability to withstand shrinkage stress (Zhu et al., 2021; Li et al., 2023; Huang, 2000).

Table 9. Drying shrinkage rate (ε_{at}/%) of samples without polycarboxylate superplasticizer.

ID	10 d	14 d	17 d	21 d	24 d	28 d	35 d	42 d	49 d	56 d
*C*4*W*52	0.27	0.57	0.99	1.12	1.18	1.19	cracking	cracking	cracking	cracking
*C*8*W*52	0.29	0.58	0.98	1.09	1.14	1.15	1.20	1.21	1.21	1.22
*C*12*W*44	0.24	0.48	0.81	0.87	0.92	0.93	0.97	0.98	0.98	0.98
*C*12*W*48	0.27	0.54	0.90	0.93	0.98	0.99	1.01	1.03	1.04	1.04

*C*12*W*52	0.30	0.60	0.98	1.03	1.08	1.09	1.10	1.11	1.11	1.11
*C*12*W*56	0.33	0.65	1.04	1.12	1.15	1.14	1.17	1.19	1.19	1.20
*C*16*W*52	0.34	0.61	0.97	0.98	1.04	1.07	1.07	1.08	1.08	1.08

As shown in Table 8, when C = 12%, drying shrinkage becomes increasingly pronounced with higher W at all ages (Kovler and Zhutovsky, 2006). Fig. 20 further illustrates that the trends of ε_{at} and w_r over time are closely correlated. During the first 17 d, high w_r leads to significant shrinkage [48]. After 17 d, hydration products partially mitigate ε_{at}. However, ε_{at} continues to increase due to water evaporation until 35 days, when w_r stabilises, causing the growth of ε_{at} to gradually slow. These findings highlight that higher W exacerbates drying shrinkage and cracking, emphasising the necessity of strictly controlling water content for engineering applications.

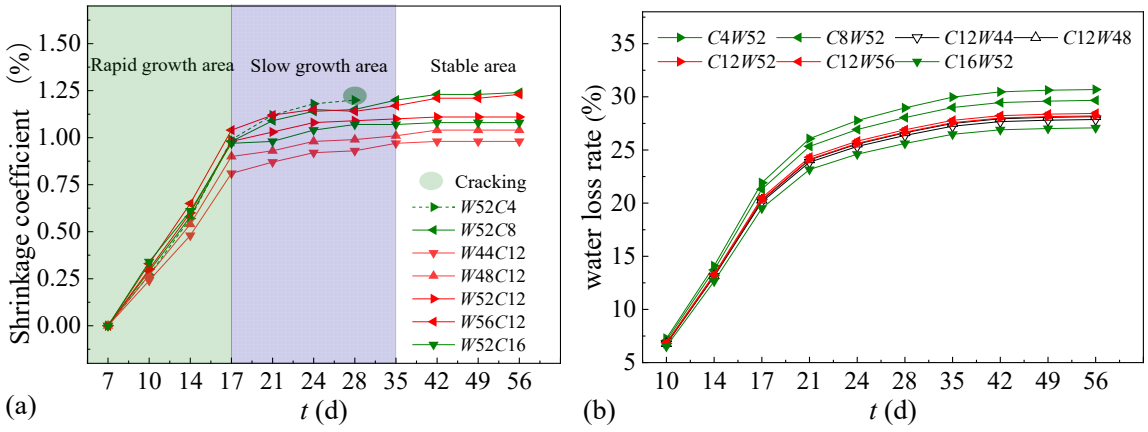

Fig. 20. Time-dependent changes: (a) drying shrinkage rates versus time; (b) water loss rates versus time.

The drying shrinkage rate ε_{at} for samples with polycarboxylate superplasticizer is shown in Table 10. At constant C and W, ε_{at} increases with P during the first 17 d. This increase occurs because the pore structure in superplasticized samples facilitates early capillary water escape (Kovler and Zhutovsky, 2006; Ma et al., 2006). Early curing is, therefore, crucial for CLSM containing polycarboxylate superplasticizer during the construction phase. At 56 d, a 0.40% increase in P results in a 0.09% reduction in ε_{at}. This is attributed to the dispersion of agglomerated large particles caused by the polycarboxylate superplasticizer, which leads to uniform and dense particle packing.

Additionally, the increased production of cement hydration products effectively fills the voids (Zhu et al., 2021; Li et al., 2023; Chen et al., 2015). Similarly, the effect of the polycarboxylate superplasticizer on ε_{at} is evaluated under the same flowability design standard. Both *C*12*W*52 and *C*10*W*46*P*0.1 samples exhibit the same flowability (255 mm), but their ε_{at} values are 1.11% and 0.97%, respectively. This indicates that under the same flowability design standard, the addition of the polycarboxylate superplasticizer reduces *W*, resulting in a more significant reduction in ε_{at} at 56 d.

Table 10. Drying shrinkage rate (ε_{at}/%) of samples with polycarboxylate superplasticizer

ID	10 d	14 d	17 d	21 d	24 d	28 d	35 d	42 d	49 d	56 d
*C*10*W*46*P*0	0.18	0.38	0.64	0.88	0.92	0.97	0.99	1.00	1.00	1.01
*C*10*W*46*P*0.1	0.22	0.4	0.66	0.86	0.9	0.95	0.96	0.97	0.97	0.97
*C*10*W*46*P*0.2	0.25	0.41	0.69	0.87	0.89	0.94	0.94	0.95	0.94	0.94
*C*10*W*46*P*0.3	0.31	0.47	0.72	0.88	0.89	0.91	0.93	0.93	0.93	0.93
*C*10*W*46*P*0.4	0.34	0.49	0.75	0.88	0.89	0.91	0.91	0.92	0.92	0.92

3.3.2 Water stability

The residual strength (q_{rs}) of samples without polycarboxylate superplasticizer after *N* wet-dry cycles is shown in Fig. 21(a). Except for sample *C*4*W*52, which disintegrated during the ninth cycle, most samples exhibited an initial increase in q_{rs}, followed by a decline, with evidence of stability after nine cycles. With the addition of the polycarboxylate superplasticizer, the trend of q_{rs} variation with the number of dry-wet cycles is similar to that of the sample without polycarboxylate superplasticizer, as shown in Fig. 21(b). During the early cycles, elevated temperatures and sufficient moisture promote cement hydration, enhancing sample strength, particularly in those with higher cement content (Ye et al., 2018; Wan et al., 2021; Zheng et al., 2009). As the cycles progress, repeated drying shrinkage and wetting expansion induce deformation stresses that exceed the structural strength, leading to stress concentration at weak points between soil particles and the formation of microcracks (Wang and Gao,

2006), as illustrated in Fig. 22. These microcracks allow water infiltration, further degrading the internal structure and reducing compressive strength (Cuisinier et al., 2020; Jiang et al., 2023). Fig. 21 also shows that, except for *C*4*W*52, the decline in q_{rs} slows after the ninth cycle. For instance, the compressive strength of the *C*12*W*48 sample reaches stability after 13 cycles. Fig. 16 shows that its stable strength is approximately 0.8 MPa, sufficient to meet the backfill requirements for bridge abutments and culvert backs. This stabilisation is attributed to internal cracks that widen after several cycles, providing space for deformation and reducing the damaging effects of shrinkage and expansion on the structure (Qian et al., 2019; Ye et al., 2018; Wang and Gao, 2006).

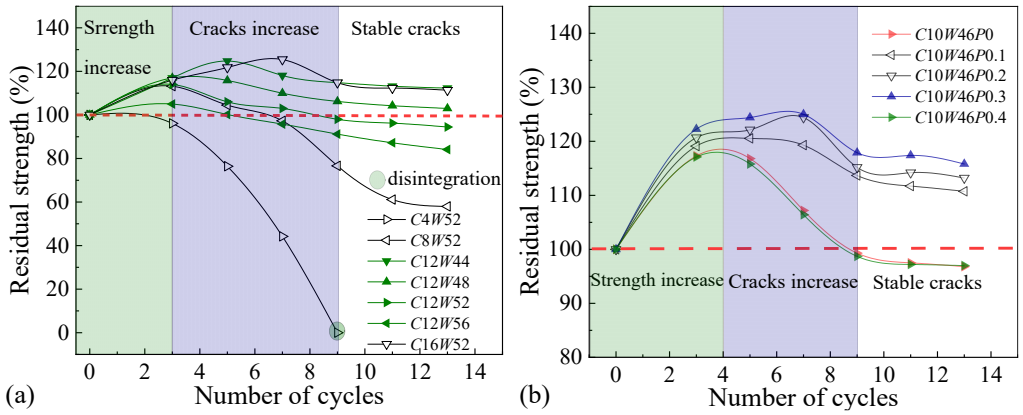

Fig. 21. Residual strength versus number of dry-wet cycles:(a) samples without polycarboxylate superplasticizer; (b) samples with polycarboxylate superplasticizer.

Fig. 21(a) demonstrates that when C = 12% and W increases from 44% to 56%, q_{rs} decreases by 26% after 13 wet-dry cycles, indicating substantial deterioration. To ensure water stability, strict limits on W are important (Liu et al., 2022). At W = 52%, increasing C significantly enhances water stability. For instance, while *C*4*W*52 disintegrates, *C*8*W*52 did not disintegrate，as illustrated in Fig. 22. This improvement is attributed to the increased cement hydration products, which reduce interconnected pores and block channels for permeability, thereby mitigating damage from wet-dry cycles, as shown in Fig. 23 (Cuisinier et al., 2020; Du et al., 2024; Liu et al., 2022). Also, as shown in Fig. 21(b), increasing the quantity of polycarboxylate superplasticizer P from 0% to 0.3% improves q_{rs} by

approximately 19% after 13 wet-dry cycles. The polycarboxylate superplasticizer enhances particle distribution, resulting in a more uniform and dense structure, while also promoting the production of ultimate cement hydration products (Ye et al., 2018; Wan et al., 2021; Zheng et al., 2009). However, excessive *P* causes severe bleeding, weakening the surface layer and generating microcracks that accelerate water infiltration and dissolution (He et al., 2020; Yu et al., 2017). Consequently, increasing P from 0.3% to 0.4% reduces q_{rs} by 18.8%. At the same flowability (255 mm), the q_{rs} of *C*12*W*52 is approximately 17% lower than that of *C*10*W*46*P*0.1 after 13 cycles of wetting and drying. This indicates that adding the polycarboxylate superplasticizer allows the sample to achieve the flowability design standard at a lower *W*, thereby improving water stability and reduces the cement required to maintain it.

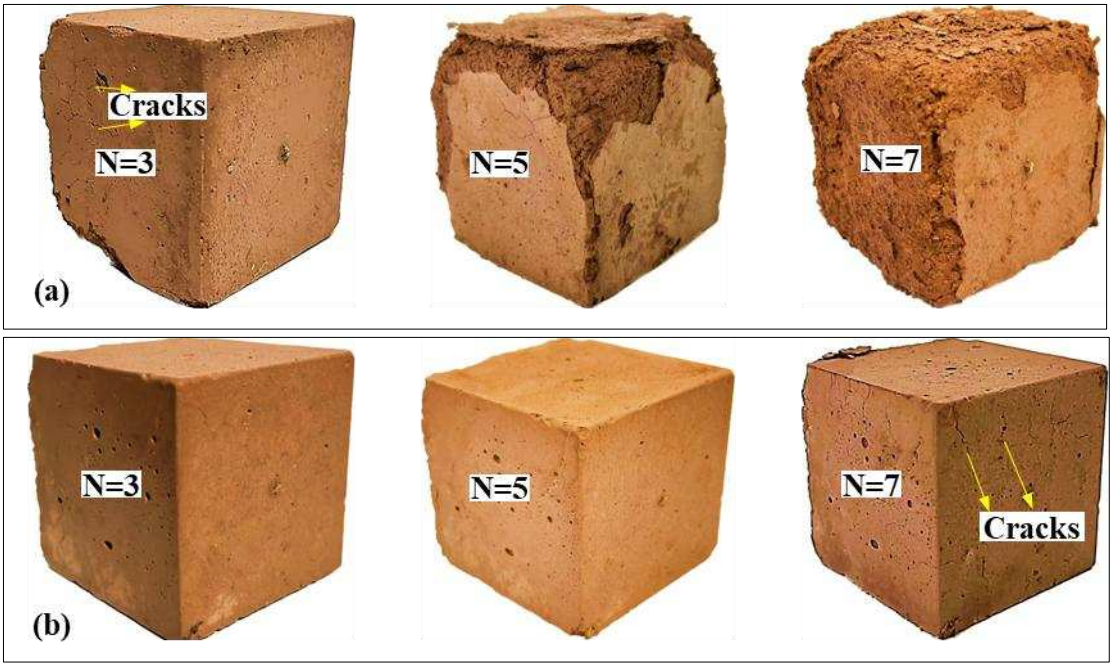

Fig. 22. Appearance of samples with different mix proportions after *N* wet-dry cycles: (a) *C*4*W*52; (b) *C*8*W*52.

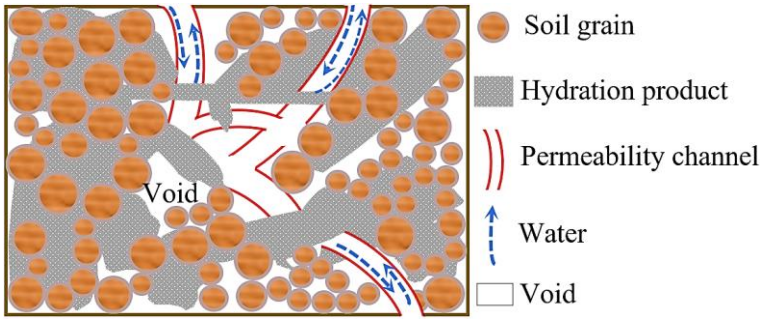

Fig. 23. Cement hydration products blocking permeability channels in CLSM samples.

4. Conclusions

This paper studied the use of waste red-bed mudstone, cement, polycarboxylate polycarboxylate superplasticizer and water to produce Controlled Low-Strength Material (CLSM). By investigating the effects of cement-to-soil ratio (C), water-to-solid ratio (W), and quantity of polycarboxylate superplasticizer (P) on the fresh, hardened, and durability properties of CLSM, the feasibility of employing red-bed mudstone as an aggregate was demonstrated. The role of polycarboxylate superplasticizer in enhancing both the performance and sustainability of CLSM was also explored. The key findings are as follows:

1. **Flowability**: The initial flowability of CLSM without the addition of polycarboxylate superplasticizer significantly increases with higher water content (W) and slightly with increased cement content (C). Using normalization, an estimation model for initial flowability as a function of C and W can be developed. For a project flowability range of 165 mm-285 mm, using 0.2% polycarboxylate superplasticizer reduces water content by 8.6%-10.2%, thus balancing water content and flowability requirements. When polycarboxylate superplasticizer is added, the flowability loss rate exhibits a logarithmic relationship with time, with an average rate of 26%-30% at 3 h.
2. **Bleeding rate**: Samples without polycarboxylate superplasticizer maintained bleeding rates below

5% within the investigated ranges of W and C. Although increasing the polycarboxylate superplasticizer dosage at constant W and C raised the bleeding rate, adjusting the mix to achieve the same flowability resulted in a 1.8% reduction in bleeding rate compared to mixes without polycarboxylate superplasticizer.

3. **Setting time**: For mixes within the range of W = 44%-56% and C = 4%-16%, the setting time can be controlled within 24 h. Adding polycarboxylate superplasticizer extended the setting time when W and C were constant. However, under the same flowability standard, its impact on setting time was minimal.
4. **Settlement rate**: CLSM settlement was influenced by bleeding and cement hydration. While polycarboxylate superplasticizer increased settlement rates at constant W and C, at the same flowability (250 mm), P of 0.1% reduced settlement rate by 1%.
5. **Compressive strength**: without the addition of polycarboxylate superplasticizer, compressive strength increased with higher C and decreased with higher W. A normalized model for compressive strength as a function of C and W was established. The addition of polycarboxylate superplasticizer allowed for reduced water content to achieve target flowability, subsequently lowering the required cement content to attain the same compressive strength. This optimization has the potential to reduce cement costs and enhance sustainability by addressing high water and cement content issues.
6. **Drying shrinkage rate**: drying shrinkage rates increased rapidly during the first 17 days and stabilized by 56 days in samples without polycarboxylate superplasticizer. The polycarboxylate superplasticizer slightly increased early-age shrinkage but reduced long-term shrinkage. Under the same flowability standard, polycarboxylate superplasticizer significantly decreased drying

shrinkage at 56 days, minimizing the risk of cracking due to high water content.

7. **Water stability:** the residual strength of CLSM initially increased during wet-dry cycles, before then decreasing and then stabilizing. Water stability improves with higher *C* but deteriorates significantly with increasing *W*. An appropriate polycarboxylate superplasticizer dosage (0.1% – 0.3%) can enhance water stability, especially when evaluated under the same flowability standard.

In summary, the combined use of waste red-bed mudstone, cement, and polycarboxylate superplasticizer in CLSM can achieve material properties suitable for a variety of engineering backfill applications. The incorporation of polycarboxylate superplasticizer reduces the water content required for target flowability, which in turn decreases bleeding rate, setting time, settlement rate, and drying shrinkage, while enhancing compressive strength and water stability. This approach resolves the inherent trade-offs between flowability and other engineering properties. Additionally, reducing the cement-to-soil ratio necessary to meet strength requirements lowers cement consumption, aligning with sustainable development goals. Future research should focus on establishing precise quantitative relationships between superplasticizer dosage, reduced cement content, and various engineering performance indicators. This would help further optimize CLSM mix designs and potentially improve the economic and environmental benefits of using waste red-bed mudstone in sustainable construction practices.

Acknowledgments

This research was funded by the Major Program of Natural Science Foundation of Sichuan Province (Grant No. 2024NSFSC0003), the Natural Science Foundation of Sichuan Province (Grant No. 2023NSFSC0391), and the Overseas Expertise Introduction Project for Discipline Innovation (“111 Project”, Grant No. B21011).

References

ACI 229 R-99, 1999. Controlled Low Strength Materials.

Aehnelt, M., Hilse, U., Pudlo, D., Heide, K., Gaupp, R., 2021. On the origin of bleaching phenomena in red bed sediments of triassic buntsandstein deposits in central germany. Geochemistry 81, 125736. https://doi.org/10.1016/j.chemer.2020.125736

Ahmed, A., Ugai, K., 2011. Environmental effects on durability of soil stabilized with recycled gypsum. Cold Reg Sci Technol 66, 84–92. https://doi.org/10.1016/j.coldregions.2010.12.004

Arm, M., Wik, O., Engelsen, C.J., Erlandsson, M., Hjelmar, O., Wahlström, M., 2017. How Does the European Recovery Target for Construction & Demolition Waste Affect Resource Management? Waste Biomass Valorization 8, 1491–1504. https://doi.org/10.1007/s12649-016-9661-7

Carrasco, F., Grathwohl, S., Maier, J., Ruppert, J., Scheffknecht, G., 2019. Experimental investigations of oxyfuel burner for cement production application. Fuel 236, 608–614. https://doi.org/10.1016/j.fuel.2018.08.135

Chang, C.-F., Chen, J.-W., 2006. Development and Production of Ready-Mixed Soil Material. J Mater Civ Eng 18, 792–799. https://doi.org/10.1061/(ASCE)0899-1561(2006)18:6(792)

Chang D., Liu J., Li X., 2015. Normalized stress-strain behavior of silty sand under freeze-thaw cycles. Rock and Soil Mechanics 36, 3500-3505+3515. https://doi.org/10.16285/j.rsm.2015.12.021

Chittoori, B., Puppala, A.J., Raavi, A., 2014. Strength and Stiffness Characterization of Controlled Low-Strength Material Using Native High-Plasticity Clay. J Mater Civ Eng 26, 04014007. https://doi.org/10.1061/(ASCE)MT.1943-5533.0000965

Chen H., Qian C., Zhao F., Qu J., Guo J., Michael D., 2015. Effect of polycarboxylate-type superplasticizer on hydration products of cement. Journal of Southeast University(Natural Science Edition) 45, 745–749.

Cheng Q., Kou X., Huang S., Zhou Y., 2004. The Distributes And Geologic Environment Characteristics Of Red Beds In China. Journal of Engineering Geology 34–40. https://doi.org/10.3969/j.issn.1004-9665.2004.01.007

Cheng Y., Wang Mi., Li G., Chen Y., Li H., 2016. Analysis On The Causes Of Landslide Of BAZHONG-NANCHONG-GUANG'AN HIGHWAY In East sichuan Of Red Beds Area. Journal of Geological Hazards and Environment Preservation 27, 1–6. https://doi.org/10.3969/j.issn.1006-4362.2016.03.001

Cuisinier, O., Masrouri, F., Mehenni, A., 2020. Alteration of the hydromechanical performances of a stabilized compacted soil exposed to successive wetting–drying cycles. J Mater Civ Eng 32, 04020349. https://doi.org/10.1061/(ASCE)MT.1943-5533.0003270

CSWADI, 2022."Technical standard for engineering application by using premixed fluidized stabilized soil"DBJ51/T 188–2022, Chengdu, China.

Deng X., Huang X., Ning J., 2011. Influence of admixture on strength of stabilized soils. Chinese Journal of Geotechnical Engineering 33, 1628–1633.

Di Bella, C., Wyrzykowski, M., Lura, P., 2017. Evaluation of the ultimate drying shrinkage of cement-based mortars with poroelastic models. Mater Struct 50, 52. https://doi.org/10.1617/s11527-016-0870-0

Du, J., 2024. Characterization of controlled low-strength materials from waste expansive soils. Constr Build Mater.

Du, J., Zhang, L., Hu, Q., Luo, Q., Connolly, D.P., Liu, K., Hu, T., Zhu, J., Wang, T., 2024. Characterization of controlled low-strength materials from waste expansive soils. Constr Build Mater 411, 134690. https://doi.org/10.1016/j.conbuildmat.2023.134690

Duan, H., Miller, T.R., Liu, G., Tam, V.W.Y., 2019. Construction debris becomes growing concern of growing cities.

Waste Manage (oxford) 83, 1–5. https://doi.org/10.1016/j.wasman.2018.10.044
H. Dalal, P., Patil, M., K.R Iyer, K., N. Dave, T., 2023. Sustainable controlled low strength material from waste materials for infrastructure applications: State-of-the-art. J Environ Manage 342, 118284. https://doi.org/10.1016/j.jenvman.2023.118284
Hu, Q., Zhang, L., Luo, Q., Yu, K., Connolly, D.P., Qin, L., Wang, L., Wang, T., 2024. Impact of polycarboxylate superplasticizer dosage on controlled low strength material flowability and bleeding: Insights from water film thickness. Constr Build Mater 447, 138145. https://doi.org/10.1016/j.conbuildmat.2024.138145
Jian, S., Cheng, C., Lv, Y., Wang, C., Tan, H., Li, B., 2022. Preparation and evaluation of high-fluid backfill materials from construction spoil. Constr Build Mater 345, 128370. https://doi.org/10.1016/j.conbuildmat.2022.128370
Khattab, S.A., Al-Mukhtar, M., Fleureau, J.-M., 2007. Long-term stability characteristics of a lime-treated plastic soil. J Mater Civ Eng 19, 358–366. https://doi.org/10.1061/(ASCE)0899-1561(2007)19:4(358)
Kim, Y., Dinh, B.H., Do, T.M., Kang, G., 2020. Development of thermally enhanced controlled low-strength material incorporating different types of steel-making slag for ground-source heat pump system. Renewable Energy 150, 116–127. https://doi.org/10.1016/j.renene.2019.12.129
Kovler, K., Zhutovsky, S., 2006. Overview and Future Trends of Shrinkage Research. Mater Struct 39, 827–847. https://doi.org/10.1617/s11527-006-9114-z
He X., Shen W., Jia Q., Liu Y., 2020. Performance Design of Self-Compacting Concrete Incorporated with Crushed Sand Based on Two-Phase Suspension System. Journal of Southeast University(Natural Science Edition) 50, 463–470.
Huang R., Liu G., Zhu Y., Zhang P., 2021. Controlled Low Strength Materials Based on Pipe Jacking Waste Soil and Their Property Influencing Factors. Tunnel Construction 41, 346–352. https://doi.org/10.3973/j.issn.2096-4498.2021.S2.044
Huang X., 2000. Strength Enhancement Effect Of Ettringite In Soil Stabilization. Journal of the Chinese Ceramic Society 299–302, 308. https://doi.org/10.14062/j.issn.0454-5648.2000.04.001
Huang X., Ning J., Guo Y., Zhu B., 2006. Effect of cement content on the structural formation of stabilized soil. Chinese Journal of Geotechnical Engineering 436–441.
Jiang P., Chen Y., Chen X., Zhang W., Li N., Wang W., 2023. Unconfined compression behavior of modified lime stabilized soil under dry wet and freeze-thaw cycles. Journal of Jilin University(Engineering and Technology Edition) 53, 1809–1818. https://doi.org/10.13229/j.cnki.jdxbgxb.20221376
Lei H., Liu T., Cheng Q., 2019. Study of Deformation Mechanism and Support Measures for High Slope of Highway in Red Bedding Areas. Highway 64, 47–53.
Liu K., Liu L., Zhang Y., 2022. Permeability and Pore Structure of Improved Isolation Wall under the Action of Dry-Wet/Freeze-Thaw Cycles. Journal of Building Materials 25, 545–550. https://doi.org/10.3969/j.issn.1007-9629.2022.05.015
Li Y., Wang Q., Zhang Q., Zhou L., Mu J., 2023. Effect of Inorganic Curing Agents on the Structure and Properties of Fluid Cured Soils. Materials Reports 37, 156–162.
Ma B., Xu Y., Dong., 2006. Establish of Drying Shrinkage Characteristics Curve of Portland Cement and Research. Journal of Wuhan University of Technology 24–26. https://doi.org/10.3321/j.issn:1671-4431.2006.04.008
Nataraja, M.C., Nalanda, Y., 2008. Performance of industrial by-products in controlled low-strength materials (CLSM). Waste Manage (oxford) 28, 1168–1181. https://doi.org/10.1016/j.wasman.2007.03.030
Pan Z., Peng H., 2015. Comparative Study on the Global Distribution and Geomorphic Development of Red Beds. Scientia Geographica Sinica 35, 1575–1584. https://doi.org/10.13249/j.cnki.sgs.2015.12.011
Paul J. Tikalsky, H. U. Bahia, T. S., 2004. Excess Foundry Sand Characterization And Experimental Investigation In

Controlled Low-Strength Material And Hot-Mixing Asphalt. Pennsylvania Transportation Institute The Pennsylvania State.

Qian, J., Hu, Y., Zhang, J., Xiao, W., Ling, J., 2019. Evaluation the performance of controlled low strength material made of excess excavated soil. Journal of Cleaner Production 214, 79–88. https://doi.org/10.1016/j.jclepro.2018.12.171

Qian, J., Shu, X., Dong, Q., Ling, J., Huang, B., 2015. Laboratory characterization of controlled low-strength materials. Materials & Design (1980-2015) 65, 806–813. https://doi.org/10.1016/j.matdes.2014.10.012

Sheen, Y.-N., Zhang, L.-H., Le, D.-H., 2013. Engineering properties of soil-based controlled low-strength materials as slag partially substitutes to portland cement. Constr Build Mater 48, 822–829. https://doi.org/10.1016/j.conbuildmat.2013.07.046

Wan, J., Feng, Y., Li, S., Zhou S., Wang, S., Du, Y., 2021. physical and mechanical characteristics of nickel-zinc-contaminated clay solidified/stabilized by a novel steel slag-based binder subjected to wetting-drying cycles. Chinese Journal of Geotechnical Engineering 43, 213–216. https://doi.org/doi:10.11779/CJGE2021S2050

Wan, X., Ding, J., Jiao, N., Zhang, S., Wang, J., Guo, C., 2023. Preparing controlled low strength materials (CLSM) using excavated waste soils with polycarboxylate superplasticizer. Environ Earth Sci 82, 214. https://doi.org/10.1007/s12665-023-10884-5

Wang, C., Li, Y., Wen, P., Zeng, W., Wang, X., 2023. A comprehensive review on mechanical properties of green controlled low strength materials. Constr Build Mater 363, 129611. https://doi.org/10.1016/j.conbuildmat.2022.129611

Wang J., Gao Y., 2006. Study on the Strength Degradation Mechanism of Cement-Soils Resulting from Dry-Wet Cycles, China. China Railway Science 23–27. https://doi.org/10.3321/j.issn:1001-4632.2006.05.005

Wang W., HUANG Y., Wang S., Peng G., Wang H., 2024. Experimental study on influence of plasticizer on fluidity of convection-solidified silt. Chinese Journal of Geotechnical Engineering 1–9. https://doi.org/10.11779/CJGE20230828

Wang Xi., 1997. Study of Rheological Properties of Clay − Cement Pastes and Their Effect Factors. Chinese Journal of Geotechnical Engineering 45–50.

Wu, J.Y., Tsai, M., 2009. Feasibility study of a soil-based rubberized CLSM. Waste Manage (oxford) 29, 636–642. https://doi.org/10.1016/j.wasman.2008.06.017

Xu Q., Tang R., 2023. Study on red beds and its geological hazards. Chinese Journal of Rock Mechanics and Engineering 42, 28–50. https://doi.org/10.13722/j.cnki.jrme.2022.0012

Yu F., Huang Y., Sun D., 2017. Modification Effect of Lime Soil and Cement Soil by Water-Reducing Agent. Journal of Building Materials 20, 283-287+309. https://doi.org/10.3969/j.issn.1007-9629.2017.02.022

Ye, H., Chu, C., Xu, L., Guo, K., Li, D., 2018. Experimental Studies on Drying-Wetting Cycle Characteristics of Expansive Soils Improved by Industrial Wastes. Advances in Civil Engineering 2018, 1–9. https://doi.org/10.1155/2018/2321361

Zhang, J., Wang, J., Li, X., Zhou, T., Guo, Y., 2018. Rapid-hardening controlled low strength materials made of recycled fine aggregate from construction and demolition waste. Constr Build Mater 173, 81–89. https://doi.org/10.1016/j.conbuildmat.2018.04.023

Zhang J., Hou D., Gao Y., 2010. Uniform driving force for autogenous and drying shrinkage of concrete. Journal of Tsinghua University(Science and Technology) 50, 1321–1324. https://doi.org/10.16511/j.cnki.qhdxxb.2010.09.015

Zhang, N., Duan, H., Sun, P., Li, J., Zuo, J., Mao, R., Liu, G., Niu, Y., 2020. Characterizing the generation and environmental impacts of subway-related excavated soil and rock in China. J Cleaner Prod 248, 119242. https://doi.org/10.1016/j.jclepro.2019.119242

Zhang, S., 2023. Utilization of waste marine dredged clay in preparing controlled low strength materials with polycarboxylate superplasticizer and ground granulated blast furnace slag. Journal of Building Engineering.

Zheng J., Yan C., Xia W., Zhang Y., Cui D., Zhou X., Zhang R., Chen Mingzhu, 2009. Experimental Study Of Influence Of Drying And Wetting Cycles On Bearing Capacity Of Improved Soil By Cmsc Soil Stabilized Agent. Chinese Journal of Rock Mechanics and Engineering 28, 3051–3056.

Zhu H., Yu F., Geng Ji., Wang X., Qin H., 2021. Strength and Volume Stability of Controlled Low-Strength Material Based on Titanium Gypsum. Mater Struct 39 40, 3644–3653. https://doi.org/10.16552/j.cnki.issn1001-1625.20210628.002.